DOI: ADD DOINUMBER HERE

# An Automatic Domain Splitting Initial Orbit Determination Technique for Short-arc Optical Measurements

*Alessia De Riz*[⋆]*, Riccardo Cipollone*[⋆†]*, Pierluigi Di Lizia*[⋆]
[⋆] Politecnico di Milano
*Via G. La Masa 34, 20156, Milan, Italy*
*Address*
riccardo.cipollone@polimi.it · alessia.deriz@mail.polimi.it · pierluigi.dilizia@polimi.it
[†]Corresponding author

## Abstract

One of the most crucial activities related to the RSO catalogue maintenance operations segment is Initial Orbit Determination (IOD), usually acting as last resort in this context. In this regard, the present work describes a novel development of the two-body integral-based IOD method, exploiting an Automatic Domain Splitting technique and Differential Algebra and relieving most of the computational burden involved. Uncertainty is included as a covariance matrix, expanded to a predefined order. The algorithm has been tested with both simulated and real data from uncorrelated measurements of GEO optical measurements, providing promising results in terms of accuracy and processing time.

## 1. Introduction

Initial Orbit Determination (IOD) acts as last resort in case the correlation process fails and a new object has to be included among the catalogued ones. Currently, diverse methods to perform this task compose a richly populated state of the art, from improved versions of traditional ones like Gauss,[1] Laplace[2] or Gooding[3] methods to more recent and robust ones such as Admissible Regions;[4] nevertheless, there is an increasing drive towards optimization and development of techniques leveraging different aspects of the problem to better suit the amount and kind of data related to sensor observations. In this regard, the present work describes a novel development of the two-body integral-based IOD method, used to extract orbital states from optical tracks, and previously applied to asteroids analysis. Usually, iterative root-finding algorithms are used to obtain the solution and consequently build a first orbit estimate. By exploiting an Automatic Domain Splitting (ADS) technique, based on a squared approximation error splitting rule, and Differential Algebra (DA), the computational burden involved in the procedure can be considerably relieved by assessing a suitable a priori level of approximation.

## 2. Fundamentals

In this section, some of the paramount tools adopted for the method development are introduced, from the two-body integral method itself[5] ,[6] to the modifications and differential algebra formulation allowing the automatic domain splitting optimizer developed for this work to overcome iteration-based ones in terms of performance. Besides, the uncertainty propagation method is addressed, underlining its deep connection to the DA formulation on which the whole method is based.

### 2.1 Two-body integral method

This technique is used to extract orbital states from optical tracks, addressing both the insertion of a new object in a catalogue and the linkage between uncorrelated tracks by defining an orbit estimate connecting them.

The whole method is based on the two-body problem integrals of motion, so the assumption of unperturbed Keplerian motion is deemed to hold across the observation arc (limiting applications in terms of observation time window or orbital regime). As a consequence, the quantities employed in the problem, namely energy $\mathcal{E}$, angular momentum vector $\mathbf{h}$ and Laplace-Lenz vector $\mathbf{L}$ are conserved. A further aspect to address consists in the fact that the measurements have to be preprocessed in the form of an attributable, given as input to the algorithm. An optical

attributable in this case is defined as a 4D vector rearranging the observation data into two angles and two angular rates $\mathcal{A} = (\alpha, \delta, \dot{\alpha}, \dot{\delta})$. Through mathematical manipulation, the mentioned constants of motion can be expressed as non-linear functions of a couple of optical attributables, leveraging their definition together with the equations linking measurements and orbital states:

$$\mathbf{r} = \mathbf{R} + \rho\,\mathbf{s} \tag{1}$$

where $\mathbf{r}$ denotes the target position, $\rho$ represents the range while $\mathbf{s}$ is defined as:

$$\mathbf{s} = \left(\cos\alpha\,\cos\delta, \sin\alpha\,\cos\delta, \sin\delta\right) \tag{2}$$

The non-linear system final form loses its dependence on range-rate thanks to a specific projection to get its coefficients to be null, resulting in:

$$\begin{cases} q(\rho_1, \rho_2) = 0 \\ p(\rho_1, \rho_2) = 0 \end{cases}, \quad \rho_1, \rho_2 > 0 \tag{3}$$

According to the formulation, $p$ may embed the $\mathbf{L}^6$ or $\mathcal{E}^5$ residual. Then sticking to the original method, Eqn. (3) is solved through the computation of the system resultant with respect to one of the two variables at play. To compute the resultant an approach based on the Discrete Fourier Transform (DFT), Inverse DFT is employed.

Therefore, the obtained solution batch shall be further analyzed to select the most suitable one, verifying its compliance to some compatibility conditions based on unexploited orbital parameters, i.e. argument of pericenter and mean anomalies:

$$\begin{cases} \omega_1 = \omega_2 \\ M_1 = M_2 + n(t_1 - t_2) \end{cases} \tag{4}$$

### 2.2 Differential Algebra

DA allows to solve analytical problems through an algebraic approach by means of the Taylor polynomials algebra. Any deterministic function $f$ of $v$ variables that is $C^{(k+1)}$ in the domain of interest $[-1, 1]^v$ (scaled according to needs) is expanded into its Taylor expansion up to an arbitrary order $k$ with limited computational effort. Thus, variables are represented as truncated power series (TPS) around an expansion point $x_0$, instead of standard types.[7] The DA framework is implemented in a $C++$ computational environment through the DACE library. The key DA features exploited are:

- The expansion of the solution of parametric implicit equations: this feature can be used to easily explore the non-linear system solution space and bound regions of interest according to given constraints.
- The flow expansion of an Ordinary Differential Equation (ODE): this feature relieve the processing burden due to iterative integrators embedding the whole integration scheme in a single function evaluation.

### 2.3 Automatic Domain Splitting

The ADS[7] tool plays a fundamental role in the proposed algorithm. It firstly detects the error that quantifies how much an $n$-order TPS diverges from the original function following Taylor's theorem: it states that the approximation error between a $k+1$ times differentiable function $f \in C^{k+1}$ and its $k$-order Taylor expansion $P_f$ comply to:

$$|f(\delta x) - P_f(\delta x)| \leq C\delta x^{k+1} \tag{5}$$

For some constant $C > 0$. As a consequence, analysing the $k+1$-order coefficients can lead to the upper bound of the mentioned error.

The tool then identifies the variable across which it peaks and splits the domain along that direction by the following re-mapping:

$$\begin{aligned} D_1(x) &= \frac{1}{2}\,x + \frac{1}{2} \\ D_2(x) &= \frac{1}{2}\,x - \frac{1}{2} \end{aligned} \tag{6}$$

Where $D_1$ and $D_2$ are the two subdomains across the split direction $x$. According to Eq. 5 this process causes the approximation error to drop of a factor of 2. By performing a sequence of splits across different directions as a series of function compositions lower order expansions can be used to reliably represent the original function as a piece-wise one. The result is a mesh of domains and their corresponding TPS, the union of which corresponds to the initial DA set.

### 2.4 Uncertainty

In an initial orbit determination framework, uncertainty propagation allows to assess the sensitivity of the estimation method on the quality of sensor measurements. Concerning the present work, the differential algebra formalism enables a smart propagation of an initial Gaussian uncertainty exploiting the DA variable structure itself. To account for non-linearities of the statistical moments (mean and covariance in particular) in the propagation and transformations in general, State Transition Tensor Propagation (STT) can be used.[8] Leveraging Isserlis' theorem, a distribution expressed in terms of mean and covariance can be used to obtain them downstream of an input non-linear function, up to a given order (closely related to the Taylor expansion one in the case at hand). More specifically, given a generic function $[y] = f([x])$ defined in a DA framework, it yields:

$$\begin{aligned}[y] &= f([x]) \\ &= \mathcal{T}^k(\delta x) \\ &= \sum_{p_1,...,p_n \leq k} c_{p_1,...,p_n}(\delta x_1^{p_1}, ..., \delta x_n^{p_n})\end{aligned} \tag{7}$$

where $c_{p_1,...,p_n}$ are the coefficients of the Taylor expansion ($T^k$) and, in this case, coincide with the STT terms:

$$c_{p_1,...,p_n} = \frac{1}{p_1!, ..., p_n!} \frac{\partial^{p_1,...,p_n} f}{\partial x_1^{p_1}, ..., x_n^{p_n}} \tag{8}$$

As a consequence, the non linear evolution of both mean and covariance can be described as function of these coefficients, and are consequently expanded to order $k$ as:

$$\begin{aligned}\mu_i &= E\{[y_i]\} \\ &= \sum_{p_1,...,p_n \leq k} c^{\mu_i}_{p_1,...,p_n} E\{\delta x_1^{p_1}, ..., \delta x_n^{p_n}\} \\ P_{i,j} &= E\{([y_i] - \mu_i)([y_j] - \mu_j)\} \\ &= \sum_{q_1,...,q_n \leq 2k} c^{P_{i,j}}_{q_1,...,q_n} E\{\delta x_1^{q_1}, ..., \delta x_n^{q_n}\}\end{aligned} \tag{9}$$

Where $c^{\mu_i}_{p_1,...,p_n}$ are the coefficient of the expansion related to the mean value $i$-th component, while $c^{P_i}_{q_1,...,q_n}$ are the ones resulting from the evaluation of $([y_i] - \mu_i)([y_j] - \mu_j)$. Being the order of expansion set a priori, it is important to highlight that the covariance order shall be double the $k$ one used for the polynomial map expansion in order to keep consistent accuracy in the approximation process.

This technique represents a generalization to a given $n$-order of the linear projection of covariance through the Jacobian of a transformation:

$$\mathbf{\Gamma}_Y = \frac{\partial \mathbf{Y}}{\partial \mathbf{X}} \mathbf{\Gamma}_X \frac{\partial \mathbf{Y}}{\partial \mathbf{X}}^T \tag{10}$$

where $\frac{\partial \mathbf{Y}}{\partial \mathbf{X}}$ is the Jacobian associated to the transformation.

## 3. Method

This section outlines how the DA-ADS based technique design process is structured (see Fig. 1). A preliminary phase has been performed to evaluate the performance, stability and feasibility of the method with standard root-finding algorithms. Phase I encloses the differential algebra transposition of the original method, exploiting polynomial inversion and domain splitting to find solution efficiently. In Phase II the uncertainty propagation problem is addressed by building a slightly different polynomial map and obtaining distributions in target domains in terms of mean and covariance.

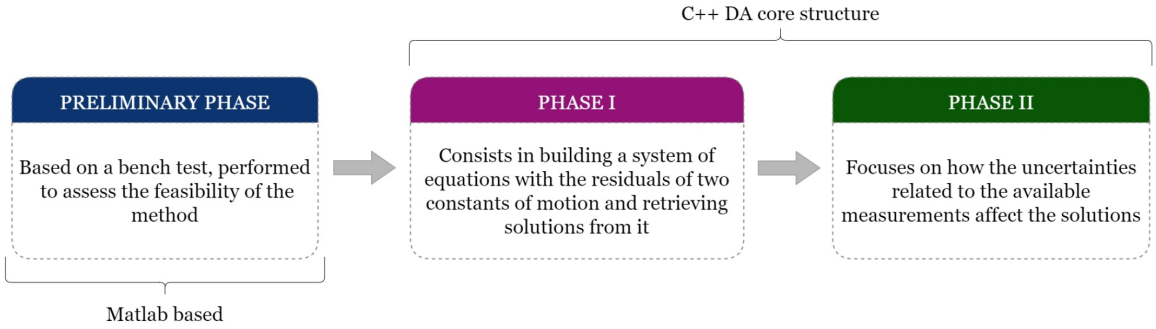


Figure 1: A workflow diagram representing the algorithm structure.

### 3.1 Preliminary Phase

The presented IOD technique basic methodology is tested in Matlab for a preliminary feasibility analysis. It is assessed by the generation of a synthetic Earth's orbit, considering the Telescope Fabra-ROA at the Montsec (TFRM) as the reference ground station providing optical measurements.

The two-body integral based IOD method is implemented in both its formulations (Energy and Lenz vector-based) to evaluate and compare their performance. Two synthetic attributables are retrieved for the non-linear system set up. Once assembled, the system is solved by means of Matlab *fsolve* routine. Different values of the input initial guess, expressed as percentages of the correct range value, have been tested to study the technique performance. The energy formulation shows a strong sensitivity to the initial guess selection (mainly due to numerical round-off errors) that prevents convergence to the correct solution. Despite tuning some of *fsolve* parameters and reaching convergence, the associated error would never lie below an acceptable threshold. Therefore, the system of equations to be developed in DA, is the one including **h** and **L** scalar residuals as it shows a more promising behaviour.

### 3.2 Phase I : Find a solution

The DACE is configured to perform the calculations up to the prescribed order and the involved independent variables $\rho_i,\ i = 1, 2$ are intialized so that an initial search space can be defined.
To equate the integrals, an approach similar to[6] is adopted. Two attributables $\mathcal{A}_i$ at epochs $t_i$, $i = 1, 2$ are considered. In order to retrieve them, given that $\dot{\alpha}_i, \dot{\delta}_i\ i = 1, 2$ are not directly acquired by the sensor, time derivatives are computed through different approaches, whether they come from synthetic measurements (using NASA SPICE kernels and functions) or real ones (by means of forward finite difference on short enough time spans).

The procedure to define the scalar residuals TPSs corresponding to specific angular momentum **h** and the Lenz-Laplace vector **L** follows a different path with respect to.[6] Since the preliminary phase highlighted struggle for convergence using the original formulation (mainly due to round-off error propagation), a more stable form of **L** expression is selected. Nonetheless, an equivalent DA form of the original system formulation can be obtained:

$$\begin{cases} [f_1] = \overline{f}_1 + \mathcal{T}_{f_1}(\delta\rho_1, \delta\rho_2) \\ [f_2] = \overline{f}_2 + \mathcal{T}_{f_2}(\delta\rho_1, \delta\rho_2) \end{cases} \tag{11}$$

Once the polynomial expansions defined in the initial domain are retrieved, the ADS comes into play. It requires an input function, defined on the original domain, that can effectively quantify the error with respect to the reference function. In this case, instead of the standard infinite norm of the residual vector, a squared sum of the two scalar residuals has been chosen to allow more splits in case of high errors:

$$g(\rho_1, \rho_2) = p^2(\rho_1, \rho_2) + q^2(\rho_1, \rho_2) \tag{12}$$

In order to reduce the significant computational burden implied with the splitting procedure (especially if a low order expansion is targeted), an upgrade to the standard ADS algorithm has been developed. Instead of splitting the entire initial domain and then searching each single sub-domain to find the system solution, this new optimized version discards all those domains definitely not containing a zero during the split procedure by means of a Polynomial Bounder routine (PB). The approximate upper and lower bounds of the two nonlinear functions can be easily computed for each subdomain being the corresponding TPS available. In this way, by virtue of the Intermediate Value Theorem,

if the limits of both $p$ and $q$ residuals within each progressively generated sub-domain are not opposite in sign, the sub-domain is discarded since it does not contain any root of the system.

Then, the final solution is searched in the set of remaining sub-domains. Starting from the polynomial expansion of $p, q$ within each sub-domain, the corresponding map is obtained by composing the splitting sequence with them:

$$\begin{bmatrix}\delta p\\ \delta q\end{bmatrix} = \begin{bmatrix}\mathcal{T}_p\\ \mathcal{T}_q\end{bmatrix}\begin{bmatrix}\delta\rho_1\\ \delta\rho_2\end{bmatrix} \tag{13}$$

They are thus inverted and evaluated for $\delta p, \delta q$ equal to zero:

$$\begin{bmatrix}\delta\rho_1\\ \delta\rho_2\end{bmatrix} = \begin{bmatrix}\mathcal{T}_p\\ \mathcal{T}_q\end{bmatrix}^{-1}\begin{bmatrix}\delta p\\ \delta q\end{bmatrix} \tag{14}$$

Yielding $\delta\rho_1, \delta\rho_2$ which are the root coordinates with respect to the expansion point of the given subdomain. Then, the obtained zero is kept or discarded depending on whether $-1 < \delta\rho_i < 1$, $i = 1, 2$ (i.e., if the currently analysed subdomain contains $\rho_1, \rho_2$).

Once the roots are retrieved, their validation is performed on Matlab by means of compatibility conditions test, so to filter unfeasible solutions out in case of multiple ones and to validate the actual ones at the same time.

### 3.3 Phase II : Uncertainty

This section of the algorithm focuses on the influence of input measurement accuracy on the initial orbit estimation process. The module aims at propagating the initial angular measurements uncertainty throughout the process to the final state estimate.

As a first step, the Gaussian uncertainty associated with angles-only measurements, which is known and denoted as a diagonal covariance matrix, has to be projected onto the space of the attributables $\mathcal{A}_1$ and $\mathcal{A}_2$, whose uncertainty is assumed Gaussian as well. The missing covariance components are the ones associated to the rotation rates. For right ascension (RA) and declination (DEC), the known sensor accuracy is taken as standard deviation $\sigma$ of the measurements leading to a $4 \times 4$ diagonal covariance matrix $\mathbf{\Gamma}_{\boldsymbol{\eta}}$ while the mean vector is $\boldsymbol{\eta}$ ($1 \times 4$). To obtain the angular velocities covariance $\mathbf{\Gamma}_{\dot{\boldsymbol{\eta}}}$ a linear covariance projection is applied. By joining both matrices an overall $8 \times 8$ block diagonal covariance matrix is retrieved.

The next step combines the DA technique with uncertainty propagation and works as follows:

1. The DACE is initialized with 10 variables (Phase I solution and angular measurements uncertainty)

$$[\rho_i] = \overline{\rho}_i + \delta\rho_i \qquad \begin{matrix}[\alpha_i] = \overline{\alpha}_i + \delta\alpha_i & [\dot{\alpha}_i] = \overline{\dot{\alpha}}_i + \delta\alpha_i\\ [\delta_i] = \overline{\delta}_i + \delta\delta_i & [\dot{\delta}_i] = \overline{\dot{\delta}}_i + \delta\dot{\delta}_i\end{matrix} \qquad i = 1, 2 \tag{15}$$

   where $\overline{\rho}_i$ are the nominal values of the solution retrieved in Phase I.

2. The map defined in Eqn. (13) is expanded by inserting the angles and their derivatives as identity matrices $\mathcal{I}$. This results in a new map, which is inverted too, yielding:

$$\delta\mathbf{y} = \mathcal{M}\delta\mathbf{x} \tag{16}$$

$$\begin{cases}\delta\mathbf{y} = [\delta\rho_i, \delta\alpha_i, \delta\delta_i, \delta\dot{\alpha}_i, \delta\dot{\delta}_i]\\ \delta\mathbf{x} = [\delta p, \delta q, \delta\alpha_i, \delta\delta_i, \delta\dot{\alpha}_i, \delta\dot{\delta}_i]\\ \mathcal{M} = [\mathcal{T}_p, \mathcal{T}_q, \mathcal{I}_\alpha, \mathcal{I}_\delta, \mathcal{I}_{\dot{\alpha}}, \mathcal{I}_{\dot{\delta}}]^{-1}\end{cases}$$

   where the submatrices $\mathcal{T}_p$ and $\mathcal{T}_q$ are the maps linking $p$ and $q$ to the attributables and the solution uncertainties. Perturbation terms around the nominal system root $\delta p$ and $\delta q$ are set to zero, so that $\delta\rho_i$ represents the problem solution uncertainty as function of the only angles perturbations. $\mathcal{M}$ is employed to link initial measurements uncertainty to the range estimates one. The input variables used as initial distribution are the angular measurements referred to both times $t_1, t_2$.

3. Given $\delta\mathbf{x}$ characterized by $\boldsymbol{\mu}$ (mean), $\mathbf{\Gamma}$ (covariance) and $\mathcal{M}$ (output map), uncertainty is propagated to $\delta\mathbf{y}$. Initializing $\delta\mathbf{x}$ as a deviation from $\boldsymbol{\mu}$ and substituting it into Eqn. (16), results in the $k$th-order Taylor expansion of $\mathbf{y}$ with respect to the initial deviation from the mean value of $\delta\mathbf{x}$, namely $[\mathbf{y}] = \mathcal{M}^k_{\mathbf{y}}(\delta\mathbf{x})$. Then, the mean value and covariance of $\mathbf{y}$ are computed making use of STT formulation.

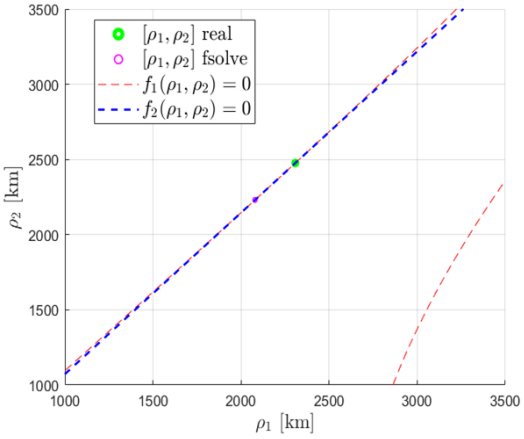


Figure 2: Energy, ideal dynamics: $\Delta t = 2$ min, contours in zero of $f_1$ and $f_2$ (dotted lines), true (green circle) and calculated (pink) solutions.

In this way, the covariance that binds the angular measurements to the solution and the corresponding mean value can be retrieved. Similarly, it is possible to link the uncertainty on angles and ranges to the states $(\mathbf{r}_i, \mathbf{v}_i)$, $i = 1, 2$ at $t_1, t_2$. Having mean and covariance of $(\rho_i, \alpha_i, \delta_i, \dot{\alpha}_i, \dot{\delta}_i), i = 1, 2$ and composing the map linking range with position, step 3 from the previous algorithm can be repeated.

Time propagation comes as the following step. To integrate the dynamics, an initial condition between the position vectors associated to $\rho_1$ and $\rho_2$ is chosen; without loss of generality, the value relative to $t_1$ is selected. Integration is performed until a selected final time $t_f$ yielding the required map projecting the initial deviation to the final state space. Combining it with the information about the initial state uncertainty, step 3 is repeated to obtain the final state mean and covariance. Subsequently, an equivalent Monte-Carlo simulation representing the actual distribution transformation is implemented to compare and validate the results of the DA-ADS based uncertainty study.

As last step, the correlation of the computed estimate with the two measurements used to generate it is performed through a Squared Mahalanobis Distance (SMD) based chi-squared test, to understand if the obtained values fall under a $3\sigma$ threshold:

$$\begin{aligned} \mathcal{SMD}(\mathbf{x}) &= (\mathbf{x} - \overline{\mathbf{x}})^T (\mathbf{\Sigma}_{\mathbf{x}} + \mathbf{\Sigma}_{\overline{\mathbf{x}}})^{-1} (\mathbf{x} - \overline{\mathbf{x}}) \\ &\sim \chi^2(\mathbf{x}) \end{aligned} \tag{17}$$

## 4. Results

Adopting the Lenz-Laplace formulation, convergence to the correct value is robust with respect to the initial condition, unlike the orbital energy version of the method which can result in convergence to wrong local minima (as can be noticed in Fig. 2).

Different case studies have been examined, taking different $\Delta t$ between the available data into account (few minutes to several hours) and applying dynamics both with and without orbital perturbations. The ideal dynamics results are not time dependent, whatever $\Delta t$ may be, the method will always converge to the correct solution. For the perturbed case, the pure Keplerian motion on which the technique relies is no longer valid thus, the obtained solution is different from the correct one. Nonetheless, it might be useful to define an equivalent Keplerian of the desired orbit to have a starting point for the results refinement.

## 5. DA-ADS

To assess the robustness of the method with respect to the length of the arc considered, the included perturbations and the TPS expansion order, the same case studies joined with supplementary ones are tested on C++.

The aim is the selection of a suitable expansion order to employ in all the simulations through a trade-off between accuracy and related computational time. Two analysis have been performed:

- Ideal dynamics (Fig. 3a): The algorithm can find a solution in any of the considered cases. The error trend between the calculated $\rho_1, \rho_2$ and the real ones, overall tends to increase with increasing expansion order (in-

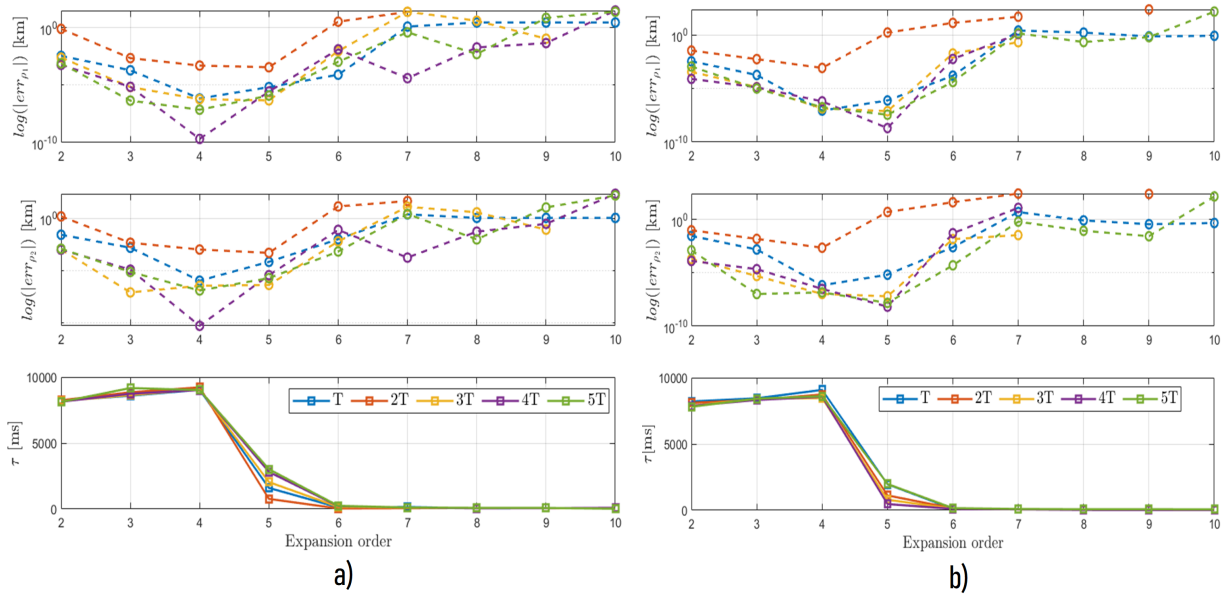


Figure 3: DA-ADS performance for, $\Delta t = kT,\ k = 1, \ldots, 5$ (T = orbital period), between the attributables.

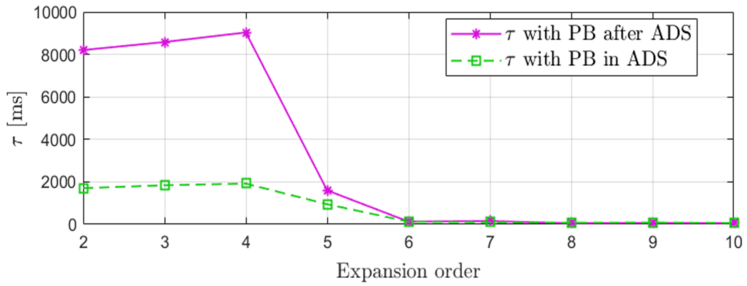


Figure 4: PB improvements on DA-ADS $\tau$

creasing non linearities and intersections between $p$ and $q$). Moreover, the low orders computational time is significantly greater because of the more generated subdomains (to comply with TPS tolerance) to scan.

- Perturbed dynamics (Fig. 3b): Similar considerations as before can be drawn. The substantial difference, is that for some high expansion order, no solution is found. This means that, the method robustness related to the expansion point selected, is drastically reduced. Nevertheless, by slightly shifting the expansion point, convergence to a solution can be achieved.

Figure 4, depicts the clear advantage of using the PB instead of the classical ADS implementation. The computational time $\tau$ of the orders up to 4 has become competitive with that of higher orders. In turn, the benefits that the higher order may have provided before are overtaken by their clear lack of stability. Therefore, the DACE will be initialized to the 4*th* order, as its computational time is rather restrained while keeping a good level of accuracy.

## 6. Real Data

For the technique validation, several batches of real observations related to GEO objects and provided by a given ground station (named STATION 1), are tested.

The outcomes of all pairs of measurements are tested to assess the results quality as the time interval and angular span of the chosen observation segment changes. The first angular measurements of the set is taken as $\mathcal{A}_1$ while $\mathcal{A}_2$ changes at each iteration spanning the remaining values.

As the time gap between the two examined measurements increases, the results quality improves. This can be appreciated thanks to the error analysis conducted on the orbital parameters $a, e$ and $\Omega$ even if they are no longer preserved in the real case (perturbations).

The blue graphs of Fig. 5 show the derived error trend between $a, e$ and $\Omega$ of the orbit obtained for $t_1$ and the correct values from a validated IOD estimate. The more the measurements are separated from each other (within a certain limit), the fewer are the possible orbits whose geometry will be able to fit the passage for the two fixed points.

As for the red graphs instead, they report the discrepancy between the same parameters, this time derived from the solutions of the method for $t_1$ and $t_2$. It can be noticed that the smaller the time interval, the smaller the effect of the perturbations whose contribution is more and more evident for increasing $\Delta t$, as shown by the increasing trends.

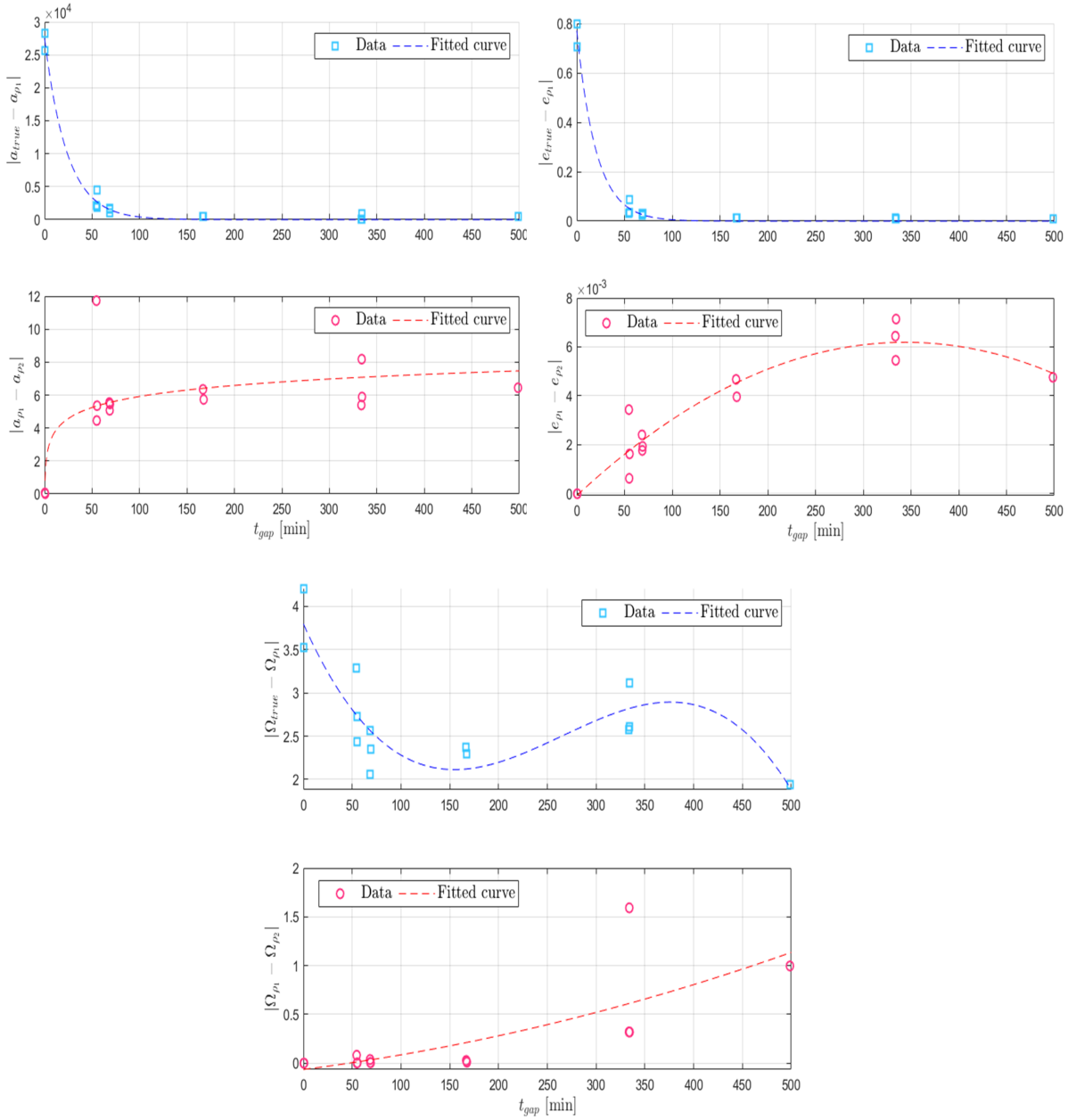


Figure 5: $a, e, \Omega$ error based on $t_2$ selected.

### 6.1 Uncertainty

After a reference couple of attributables $\mathcal{A}_1$ and $\mathcal{A}_2$ is selected, their uncertainty is propagated throughout the whole pipeline as previously outlined.

By such process, a region of orbital parameters can be defined as the one containing the initial orbit estimate, to be progressively reduced as new tracks are correlated to the two originating attributables.

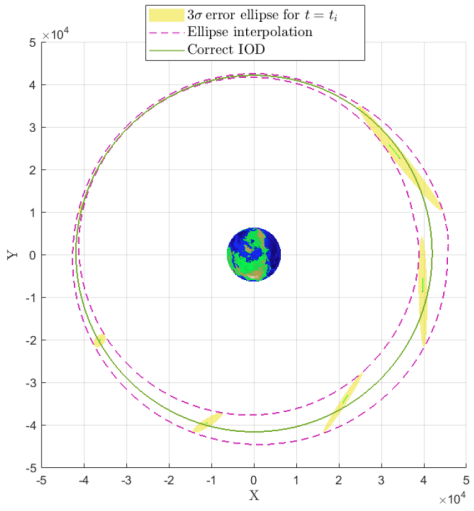


Figure 6: DA-based uncertainty assessment on **r**, **v**.

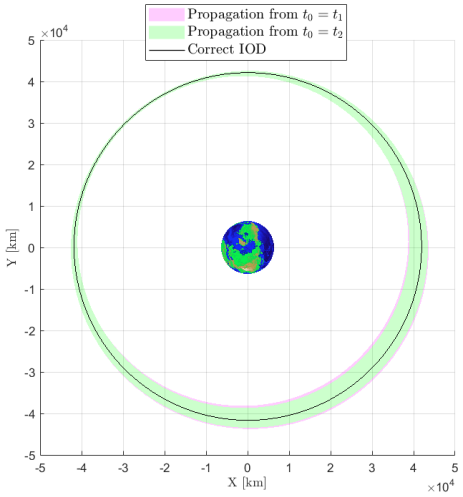


Figure 7: MC-based uncertainty assessment on **r**, **v**.

Fig. 6 shows this very region (delimited by dotted lines), retrieved as an interpolation of ellipses from the DA-based uncertainty propagation process (thus a Gaussian approximation of the actual one) that, taking measurements uncertainty into account and propagating it through state determination and propagation of dynamics, manages to include the reference orbit estimate obtained from the verified IOD. This domain is bounded by the $3\sigma$ confidence region ellipses, for n = 7 reference temporal instants.

The corresponding Monte Carlo (MC) simulation validates the approximation as shown in Fig. 7. The same approach also allowed to perform further uncertainty assessments on the employed constants of motion **h** and **L**, as shown in Fig. 8 and Fig. 9.

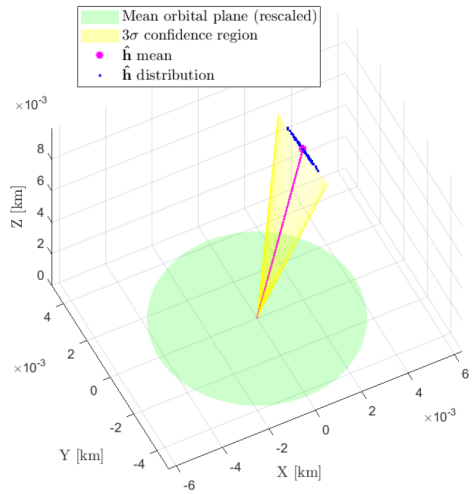


Figure 8: DA-based uncertainty assessment on **h** compared with its MC distribution.

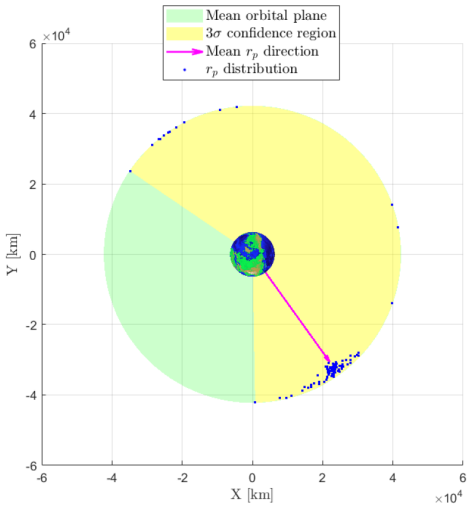


Figure 9: DA-based uncertainty assessment on $r_p$ direction compared with its MC distribution.

### 6.2 Compatibility

In order to prove if the orbit determination routine has succeded in giving a meaningful estimate, compatibility between the states corresponding to both observation times has to be tested. This can be done by leveraging the orbital parameters used throughout the process itself to compute two of the remaining ones, i.e. argument of pericenter $\omega$ and mean anomaly $M$ that, under pure Keplerian motion assumption, are supposed to comply to:

$$\begin{cases} \omega_1 = \omega_2 \\ M_1 = M_2 + n\,(t_1 - t_2) \end{cases} \tag{18}$$

Where $n$ denotes the mean motion $\sqrt{\frac{\mu}{a^3}}$ that should be the same for both orbits as well. Specific orbital energy $E$ can be taken into account too as further compatibility metric. The mentioned conditions are not likely to be satisfied in a real case scenario due to errors involving both observations and orbital perturbations between them, as shown in Fig. 10 where they are computed as function of the time difference between the two chosen observations from STATION 1. Nonetheless, they can be used in case of multiple solutions to filter out the ones largely violating them, storing a lower number of orbit hypotheses.

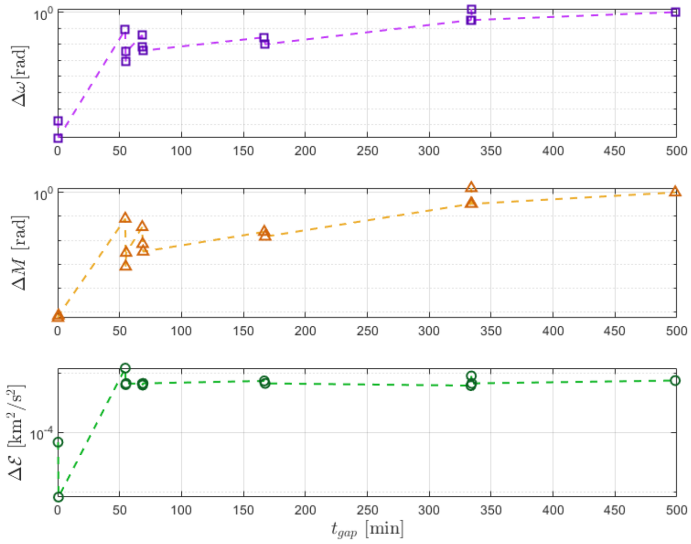


Figure 10: Residuals on $\omega$, $M$ and $E$ expressed as function of time gap between observations.

A further basic test to perform is correlation with the originating measurements. To perform this task, the Squared Mahalanobis distance is employed, enabling to define a difference between distributions to be compared with a standard known one. In particular, the aim is to define the statistical distance between the predicted $\mathbf{x}$ and the true $\overline{\mathbf{x}}$ angular measurements related to $t_2$:

$$\mathcal{SMD}(\mathbf{x}) = (\mathbf{x} - \overline{\mathbf{x}})^T (\mathbf{\Sigma}_{\mathbf{x}} + \mathbf{\Sigma}_{\overline{\mathbf{x}}})^{-1} (\mathbf{x} - \overline{\mathbf{x}}) \tag{19}$$

By comparing it with the $\chi^2(n_x)$ quantile, having a confidence level $\alpha_L = 0.998$, corresponding to $3\sigma$, and $n_x = 4$ degrees of freedom, correlation is confirmed if the $\mathcal{SMD}(x)$ is smaller than the quantile, meaning that the distance lies inside the standard gaussian stemming from the involved uncertainties:

$$\chi^2(n_x, \alpha_L) = 16.924 > \mathcal{SMD}(x)$$

Tab. 1 shows a comparison between SMD obtained from both MC simulation and DA-based covariance propagation, acting as further validation of both estimation and uncertainty propagation methods.

| $t_{gap}$ [h] | $\mathcal{SMD}(x)$ | |
|---|---|---|
| | Classic MC | DA-ADS |
| 0.91 | 6.812 | 4.536 |
| 2.78 | 16.524 | 15.852 |
| 5.57 | 2.915 | 3.784 |
| 8.31 | 0.2056 | 0.3786 |

Table 1: SMD values from the MC and DA-ADS simulations.

## 7. Conclusions

The analysis has provided promising results in terms of accuracy and significant improvements in terms of processing time thanks to ADS and subdomains pruning via polynomial bounder. Despite not yet being able to decrease errors if arcs are too short, the inclusion of measurements uncertainty allows the definition of an orbit region within which the target one should be included from the beginning. This can be used as a preliminary estimate, to be progressively shrunk with further measurements in an Orbit Determination Refinement process. Both compatibility conditions and track correlation have been verified with neighbour samples from available observations, leveraging an adequate covariance propagation procedure and proving the reliability of the IOD process. It is worth mentioning that this is the first step of a current research activity aiming at further reducing processing times by novel domain splitting and selection techniques and extending the application of the method to higher orbital regimes, as required by the rise of an operative Cislunar Space Environment.

## References

[1] J.O. Cappellari A.C. Long. Chapter 9 - Launch and Early Orbit Methods. In *Goddard Trajectory Determination System (GTDS), Mathematical Theory*, pages 9–9. Oxford, 1989.

[2] R. Danchick. Improved laplace earth satellite orbit determination using line-of-sight projective coordinates. *Journal of Spacecraft and Rockets*, 56(1):146–157, 2019.

[3] Jeremy Davis Troy A. Henderson, Daniele Mortari. Modifications to the gooding algorithm for angles-only initial orbit determination. In *American Astronomical Society Meeting 238*, 2010.

[4] De Micheli Vitturi M. Milani A., Gronchi G. Orbit determination with very short arcs. i admissible regions. *Celestial Mechanics and Dynamical Astronomy*, 12(12), 2003.

[5] G F Gronchi, L Dimare, and A Milani. Orbit determination with the two-body integrals. *Celestial Mechanics and Dynamical Astronomy*, 107(3):299–318, 2010.

[6] G F Gronchi, D Farnocchia, and L Dimare. Orbit determination with the two-body integrals. ii. *Celestial Mechanics and Dynamical Astronomy*, 110(3):257–270, 2011.

[7] A Wittig, P Di Lizia, R Armellin, K Makino, F Bernelli-Zazzera, and M Berz. Propagation of large uncertainty sets in orbital dynamics by automatic domain splitting. *Celestial Mechanics and Dynamical Astronomy*, 122(3):239–261, 2015.

[8] K Fujimoto, D J Scheeres, and K T Alfriend. Analytical nonlinear propagation of uncertainty in the two-body problem. *Journal of Guidance, Control, and Dynamics*, 35(2):497–509, 2012.